Functional alteration of brain network in schizophrenia: An fMRI study based on mutual information

Zhong-Ke Gao[1], Xin-Rui Liu[1], Chao Ma[1], Kai Ma[2], Shuang Gao[3] and Jie Zhang[4]

[1] *School of Electrical and Information Engineering, Tianjin University - Tianjin 300072, China*
[2] *Tencent Youtu Lab, Malata Building, 9998 Shennan Avenue - Shenzhen 518057, China*
[3] *First Teaching Hospital of Tianjin University of Traditional Chinese Medicine - Tianjin 300193, China*
[4] *Institute of Science and Technology for Brain-Inspired Intelligence, Fudan University - Shanghai 200433, China*

Abstract – Schizophrenia is a severe psychiatric disorder with complex neural mechanisms. Previous functional magnetic resonance imaging (fMRI) studies of schizophrenia often focused on single brain regions or selected networks. In recent years, neurophysiological alterations of schizophrenia are thought to be related with connectivity between distinct brain functional regions. The present study attempted to explore the alterations of resting-state functional connectivity to understand the neural mechanisms for adults with schizophrenia comprehensively. Here we perform a whole brain data-driven functional network analysis using resting-state fMRI data of 128 schizophrenia patients and 103 matched healthy controls. A whole brain large-scale graph theory based network is constructed using the mutual information method instead of the traditional correlation method. Significant nodal differences of network measures are found at several regions including the prefrontal cortex, hippocampus, temporal gyrus between patients and controls. Furthermore, we construct a pathological subnetwork and find intra-subnetwork edge strength differences located at the bilateral orbital gyrus and right hippocampus and the connection within temporal gyrus. Motif analysis reveal the network topological reorganization in schizophrenia happens mainly at the frontal, anterior cingulate gyrus and parahippocampal gyrus. These findings may help understand the neural basis more comprehensively and serve as a potential diagnosis marker in schizophrenia clinical application.

Introduction. – Schizophrenia is a severe psychiatric disorder characterized by abnormality delusion, hallucinations and cognitive deficits mainly regarding working memory. In recent years, based on neuroimaging data, researchers suggested that neurodevelopmental abnormalities were one of the major causes of schizophrenia [1]. Different neuroimaging studies especially magnetic resonance imaging (MRI) studies have found plenty of cortical changes in schizophrenia. Among those findings, most structural and functional neuroimaging studies indicated the crucial roles for the dorsolateral prefrontal cortex (DLPFC), thalamus, precuneus and other related regions in the pathophysiology of schizophrenia [2–5]. Based on resting-state MRI, researchers also found functional network level alterations, including default mode network [6], salience network [7] and other intrinsic networks [8].

Complex network theory [9–13] has contributed greatly to the analysis of EEG [14,15] and fMRI [16–18],

researchers have applied it in brain network and achieved much progress. Studies led to the hypothesis that the smooth functioning of brain relies on the coordination of distant brain regions, which subsequently form a subnetwork and the whole brain network, and that brain disorders are related with a lack of such coordination. Different network topological measures are found with changes in schizophrenia patients. On the structural cortical network, patients demonstrated decreased nodal centrality in several regions of the default network [16], and the network's small-worldness is damaged mainly at frontal and temporal regions [17]. On the white matter structural network, researchers found that the network hub regions' rich club organization is impaired because of the connections among frontal, parietal and insular regions [18].

The previous functional network approach usually defined the linear correlation relationship between two brain

regions as the edge strength. From all possible bivariate measures of association, linear correlation such as Pearson correlation is clearly a method of first choice, reflecting the assumption that the relationship between the functional magnetic resonance imaging (fMRI) time series can be suitably approximated by a multivariate Gaussian white noise process. As we know, hemodynamic nonlinearities could affect the blood oxygenation level-dependent (BOLD) fMRI signal [19], and the nonlinear dependence of resting-state fMRI time series has been studied [20]. Since the linearity assumption might be oversimplified, several researchers have applied nonlinear measures to measure resting-state functional connectivity [21,22], but few studies have combined graph-theory–based complex network analysis with nonlinear techniques to illustrate the network level dysfunction of schizophrenia. Here we apply the nonlinear method mutual information (MI), a concept in information theory which measures the transmission of information between two discrete time series, and has been used in fMRI functional networks construction before [23,24].

In the present study, we first construct a whole brain functional network applying the nonlinear time series analysis technique based on resting-state fMRI data, and we find functional regions with network level damage and the connectivity alteration between the nodes. Then, based on the network topological parameters, we intend to find a particular pathological subnetwork of schizophrenia to analyze and explain the healthy and disease group. Moreover, we conduct a motif analysis to illustrate the network topological reorganization in schizophrenia.

Participants, fMRI data acquisition and image preprocessing. – In our study, 231 Chinese subjects are involved, 128 of whom are schizophrenia patients (ages 24.11 ± 8.22, 73 males), and the remaining 103 are the control group (ages 24.35 ± 6.32, 47 males). Detailed demographics of the subjects are provided in table 1. This study is approved by the Institutional Review Board (IRB) of the Shanghai mental health center. All subjects agreed to participate in this experiment and signed a written consent.

The diagnoses are made by experts of psychiatrics and all patients were confirmed as schizophrenic by at least 6 months of follow-up. Symptom severity is assessed by the Positive and Negative Syndrome Scale (PANSS). Clinicians assess all healthy controls according to the DSM-IV criteria and determine that they do not have schizophrenia or other Axis I disorders, neurological disorders, head trauma, or substance dependence. All subjects receive an 8 minutes resting-state fMRI scanning, and are asked to relax with eyes closed and think about nothing in particular during the whole scan. The imaging acquisition protocol of the BOLD fMRI is obtained with a 3T General MRI system (EXCITE) using a gradient-echo echo-planar imaging (EPI) sequence (TR/TE: 2000/30 ms, flip angle 90°, slice thickness 5 mm (no gap), in-plane resolution

$3.75 \times 3.75\,\mathrm{mm}^2$, matrix size 64×64, FOV $240 \times 240\,\mathrm{mm}^2$, slices 30).

fMRI data are preprocessed using FSL [25] (`https://fsl.fmrib.ox.ac.uk/`) and AFNI [26] (`https:// afni.nimh.nih.gov/`). Images of each participant are corrected for slice timing and motion with 24 head movement parameters (6 motion parameters, 6 temporal derivatives, 6 quadratic terms, and 6 quadratic expansions of the derivatives of motion estimates for a total 24 regressors). We register functional images to a 3 mm standard Montreal Neurological Institute (MNI) space by firstly aligning functional images to the subject's T1 structural images and then transforming them to the standard space. The functional volumes are spatially smoothed with a Gaussian kernel (6 mm full width at half maximum (FWHM)). Wavelet despiking is applied to denoise the time series of voxels, and we band-pass filter the time series between 0.01 and 0.1 Hz using AFNI. White matter signal, cerebrospinal fluid signal and global mean signal are also regressed out. 94 regional time series whose length is 240 are extracted by averaging voxel time series within each anatomically defined region using the Automated-Anatomical-Labeling 2 (AAL2) template [27].

Functional network construction and subnetwork analysis. – Our basic idea is as follows: we first regard 94 brain regions divided by the AAL2 template as nodes, then determine edges in terms of mutual information between all pairs of regional BOLD signals, and finally we establish a whole-brain functional network and apply it to further analysis. In probability theory and information theory, mutual information is a measure of the interdependence of variables. Two variables' mutual information, for example $X = \{x_i\}_{i=1}^l$ and $Y = \{y_i\}_{i=1}^l$, can be mathematically defined as

$$I(X,Y) = H(X) + H(Y) - H(X,Y), \qquad (1)$$

where $H(X)$ and $H(Y)$ are the Shannon entropy of X and Y respectively, and the combination entropy of X and Y is $H(X,Y)$. The normalized result of $I(X,Y)$ can be expressed as

$$\tilde{I}(X,Y) = \frac{I(X,Y)}{\sqrt{H(X) * H(Y)}}. \qquad (2)$$

In order to compute $H(X)$ and $H(Y)$, take X as an example, we split the time series X into $n = \lfloor l^{1/3} \rfloor$ parts with the same width d. The length of the j-th interval can be expressed as

$$C_j^x = \begin{cases} [X_{\min} + d * (j-1), X_{\min} + d * j], \\ \qquad\qquad\qquad j = 1, 2, \ldots, n-1, \\ [X_{\min} + d * (j-1), X_{\max}], \quad j = n. \end{cases} \qquad (3)$$

Then for each interval $p(C_j^x)$, its probability distribution can be expressed as

$$p(C_j^x) = \frac{\text{Number of points in } C_j^x}{\text{Total number of points, } i.e., \ l} \qquad (4)$$

Table 1: Demographic and clinical characteristics of participants.

Characteristic	Controls ($N = 103$) M $\pm$ SD	Patients ($N = 128$) M $\pm$ SD	Significance T-value/χ^2	P-value
Age	24.35 ± 6.32	24.11 ± 8.22	0.06	0.807
Gender	$47\,\mathrm{M}/56\,\mathrm{F}$	$73\,\mathrm{M}/55\,\mathrm{F}$	2.97	0.085
Education	12.78 ± 3.05	11.59 ± 2.75	9.60	0.002
Illness duration		27.01 ± 22.55		
PANSS positive symptoms		20.48 ± 5.66		
PANSS negative symptoms		14.83 ± 6.76		
PANSS total psychopathology		75.90 ± 13.69		

and finally, we can figure out $H(X)$ and $H(X,Y)$ separately:

$$H(X) = -\sum_j p(C_j^x)\log_2 p(C_j^x), \tag{5}$$

$$H(X,Y) = -\sum_j \sum_k p(C_j^x, C_k^y)\log_2 p(C_j^x, C_k^y), \tag{6}$$

where $j, k = 1, 2, \ldots, n$, $p(C_j^x, C_k^y)$ means the joint probability distribution of X and Y.

When constructing the whole brain complex network, previous researches usually calculate the adjacency matrix with a sparsity around 10% to 30% [28], and to get a representational result, we carry out further analysis with a sparsity of 20%. Based on the function connection matrix of each subject, weighted and undirected network measures include the clustering coefficient (Cp) and the shortest path length (d_{ij}) is calculated. The calculation process of these network measures is as follows [29].

The clustering coefficient can be defined as

$$Cp^w = \frac{1}{n}\sum_{i \in N} \frac{2t_i^w}{k_i(k_i - 1)}, \tag{7}$$

where $k_i = \sum_{j \in N} w_{ij}$ is the weighted degree of i, $t_i^w = \frac{1}{2}\sum_{j,h \in N}(w_{ij}w_{ih}w_{jh})^{1/3}$ is the geometric mean of triangles around i. The shortest path length between i and j is

$$d_{ij}^w = \sum_{a_{uv} \in g_{i \leftrightarrow j}^w} f(w_{uv}), \tag{8}$$

where f is a map from weight to length and $g_{i \leftrightarrow j}^w$ is the shortest weighted path between i and j. In particular, since the shortest path length is an edge-specific measure, we average 94 shortest path length values under each node to transform them into nodal measures.

We then compare the network measures between patients and control group by using one-way ANCOVA, and join subject information including age, gender and education level (years) as covariates while performing the significance analysis. By analyzing the group differences between patients and control group, we separately extract a group of brain regions with significant differences under the network measures of clustering coefficient and the shortest path length ($p < 0.05$, FDR corrected). To discover the connection alterations, we choose brain regions found in the network measures mentioned above to set up a subnetwork. Functional connectivity is defined as the mutual information of each node pairs. Then all the edges differences in subnetwork are compared between the two groups, and the Bonferroni correction is used for multiple comparisons.

In the case of 20% sparsity, the obtained significant brain regions with different network measures are shown in fig. 1, and the specific significance level of each brain region is shown in fig. 2. Regarding the measure of clustering coefficient, brain regions such as right precentral gyrus (PreCG) ($p = 0.002$), bilateral precuneus (PCUN) (L: $p = 0.001/R$: $p = 0.004$) and right paracentral lobule (PCL) ($p = 0.002$) show significant differences between patients and control group. Both network measures find that several temporal lobe areas including the left superior temporal gyrus (STG) ($p = 0.008$), bilateral superior temporal gyrus of temporal pole (TPOsup) (L: $p = 0.007/R$: $p = 0.004$), right middle temporal gyrus (MTG) ($p = 0.001$) and bilateral middle temporal gyrus of temporal pole (TPOmid) (L: $p = 0.0001/R$: $p = 0.004$) show significant differences in patients. Besides, brain regions like the bilateral rolandic operculum (ROL) (L: $p = 0.002/R$: $p = 0.002$), left olfactory cortex (OLF) ($p = 0.003$), right medial orbital gyrus (OFCmed) ($p = 0.003$), left posterior orbital gyrus (OFCpost) ($p = 0.005$), bilateral hippocampus (HIP) (L: $p = 0.002/R$: $p = 0.003$), right parahippocampal gyrus (PHG) ($p = 0.003$), bilateral amygdala (AMYG) (L: $p = 0.0008/R$: $p = 0.0002$), left inferior occipital gyrus (IOG) ($p = 0.007$), left postcentral gyrus (PoCG) ($p = 0.008$) and left paracentral lobule (PCL) ($p = 0.002$) are also found with differences due to the network measure of the shortest path length between the two groups. All the brain regions' significance mentioned above has passed the FDR correction.

According to the above study, 23 different brain regions are selected through the network measures of clustering coefficient and shortest path length. A group
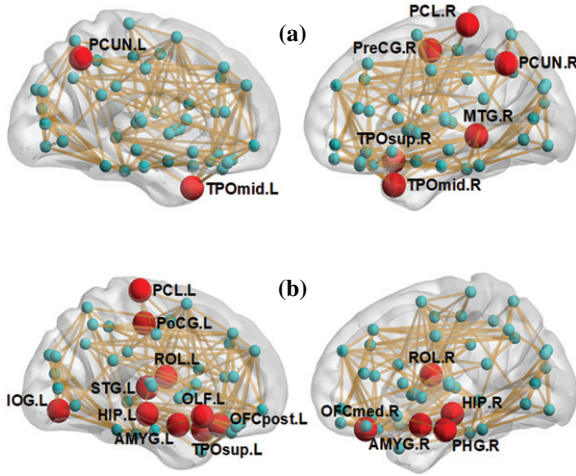
Fig. 1: Distributions of nodes showing significant network parameters differences ($p < 0.05$) at the sparsity of 20%. (a) The nodes with significant differences of clustering coefficient between two groups. (b) The nodes with significant differences of the shortest path length between the two groups. (PreCG: precental gyrus; ROL: rolandic operculum; OLF: olfactory cortex; OFCmed: medial orbital gyrus; OFCpost: posterior orbital gyrus; HIP: hippocampus; PHG: parahippocampal gyrus; AMYG: amygdala; IOG: inferior occipital gyrus; PoCG: postcentral gyrus; PCUN: precuneus; PCL: paracentral lobule; STG: superior temporal gyrus; TPOsup: temporal pole, superior temporal gyrus; MTG: middle temporal gyrus; TPOmid: temporal pole, middle temporal gyrus).

of edge information including all patient characteristics is extracted and compared with the control group for significance analysis, and demographic information is introduced as covariate. Through the above analysis, the differences between the patients and the control group in brain interval connectivity are reflected including right OFCmed with right PHG ($F = 15.16$, $p = 0.00013$) and left IOG ($F = 14.83$, $p = 0.00015$); left OFCpost with right HIP ($F = 18.17$, $p = 0.00003$), right PHG ($F = 16.78$, $p = 0.00006$) and right AMYG ($F = 17.53$, $p = 0.00004$); right HIP with left IOG ($F = 14.59$, $p = 0.00017$); left TPOsup with right TPOsup ($F = 22.64$, $p = 0.000003$) and right TPOmid ($F = 19.4$, $p = 0.00002$); and left TPOmid with right TPOmid ($F = 15.55$, $p = 0.00011$). All the significances mentioned above have passed the Bonferroni correction. The constructed subnetwork diagram is shown in fig. 3.

In the present results, we find several nodes with regional topological changes in patients, *e.g.*, bilateral precuneus, bilateral hippocampus and bilateral amygdala. In previous studies, the precuneus was consistently identified as a brain network hub both on structural networks and functional networks [30]. It is thought to be involved in many high-level cognitive functions, such as episodic memory, self-related information processing, and various aspects of consciousness [31], and analysis on schizophrenia patients has revealed hypoactivation but increased
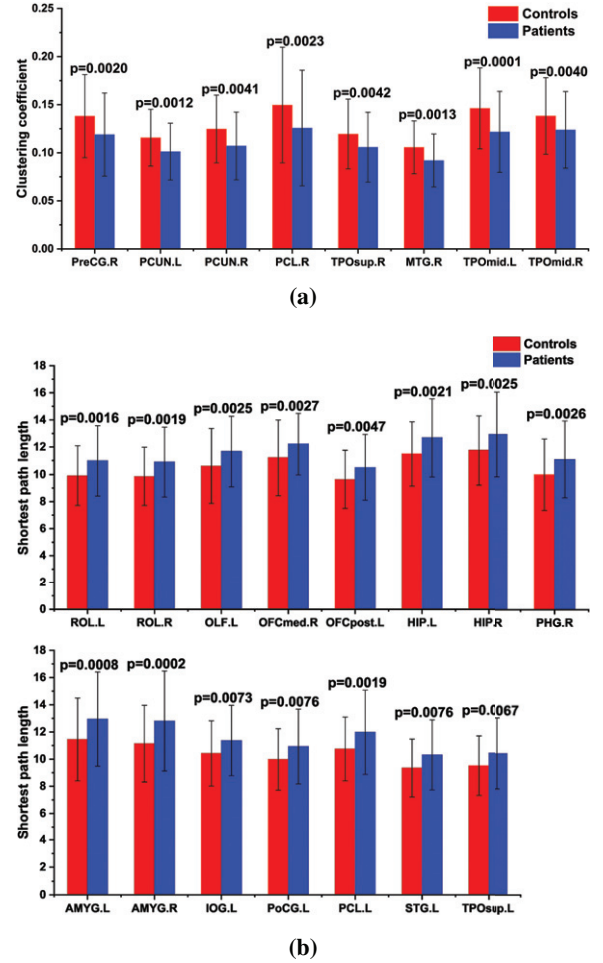

Fig. 2: The histogram of the mean and standard deviation of the network measures. (a) The nodes with significant differences of the clustering coefficient between the two groups. (b) The nodes with significant differences of the shortest path length between the two groups.
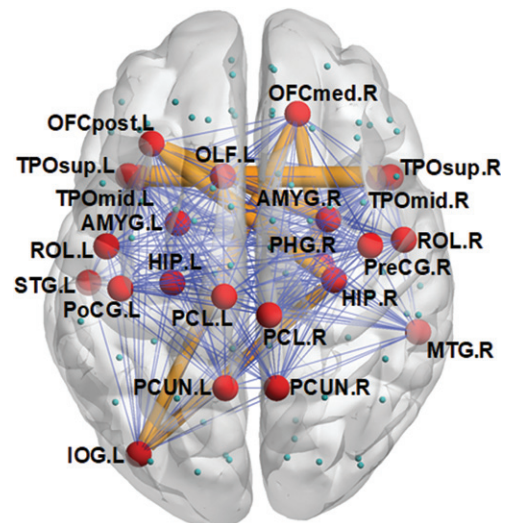

Fig. 3: Significant differences of intra-subnetwork connectivities between the two groups. The size of the edges indicates the significance of the differences of the two groups.

perfusion in bilateral precuneus which may lead to insight and metaphor comprehension ability increase in some of the patients [32,33]. The hippocampus, as the brain network communication hub for memory, plays a key role in the storage of short-term memory and the production of long-term memory [34]. Many researches demonstrated that hippocampal volume decreases in schizophrenia, and previous neuroimaging studies have revealed a pattern of increased hippocampal activity at the baseline and decreased recruitment during the performance of memory tasks in schizophrenia patients [35]. The hippocampus dysfunction is thought to be related with the dopamine system and stress [36]. Moreover, stress can also lead to amygdala activation [37], which also showed alteration in the present results. Limbic structures including hippocampus, parahippocampal gyrus and amygdala participate in the regulation of human emotions, and their dysplasia also plays a key role in schizophrenia. Limbic structures interference contributes to poor gesture performance and results in poor social functioning in schizophrenia [38], and a recent study showed a link between emotional processing deficits and limbic and prefrontal cortex systems in schizophrenia [39].

Integrating most of the current literature based on fMRI research, it can be found that functional brain networks impairment of schizophrenia patients has demonstrated reduced clustering, reduced small-worldness, increased global efficiency and increased characteristic path length [23]. Previous studies constructing whole-brain functional networks based on the Pearson correlation have found many abnormal brain regions in schizophrenia, such as the occipital lobe, orbital frontal cortical and superior temporal gyrus revealed by the clustering coefficient [40,41], and significantly longer shortest path length in frontal and temporal regions. Frontal hubs also showed a significant reduction in betweenness centrality [17]. In our study, by using mutual information to establish the functional network, a more comprehensive sample of brain abnormalities of patients are obtained through network measures analyses. The path length of a node describes how close it is connected to long distance nodes of the network; while shorter path lengths reflect a higher efficiency in transferring information [42], our findings suggest an increased path length, therefore reduced global efficiency of frontal, temporal, and occipital brain regions in schizophrenia. Besides the length path changes, current results also show nodes alterations on clustering coefficient, which characterize nodal efficiency with its neighbors. Taken together, our findings reveal that schizophrenia influenced the topological organization of the brain network on both general connectivity strength and local organization.

Some researchers studied changes in schizophrenia by analyzing the default network which includes the medial prefrontal cortex extending to ventral anterior cingulate cortex, the posterior cingulate cortex extending to the precuneus, and lateral parietal cortex [6,43]. Also the abnormal connection of salience network, between insula and DLPFC, bilateral visual cortex and insula in patients with schizophrenia was observed [7]. According to our study we find in the subnetwork that node properties around the orbital gyrus and temporal pole have changed dramatically. The frontal lobe is thought to show functional abnormalities at the onset of schizophrenia. Cortical surface size and gamma-aminobutyric acid neuron density of orbital frontal cortex vary in patients [44]. Similarly, researchers also found decreased gray matter volumes in temporal pole by comparing first-episode schizophrenia with healthy control [45]. Our subnetwork does not correspond to any specific intrinsic network, but includes some of the nodes in these networks, indicating that the brain network changes in schizophrenia exist in multiple intrinsic networks at the same time, and our graph-based approach can well explain this phenomenon in another perspective.

Motifs analysis of brain networks for characterizing schizophrenia. – In a further study, we calculate motifs to analyze brain network abnormalities between patients and control groups. Structural motifs based on the structural characteristics are one of the most common definition which form the physical substrate for a repertoire of distinct functional modes of information processing in neuronal networks. The motif fingerprint which expresses the number of distinct structural motifs of size $M = n_h$ can be mathematically defined as

$$F_{n_h}(h') = \sum_{i \in N} F_{n_h,i}(h') = \sum_{i \in N} J_{h',i}, \qquad (9)$$

where h' is any n_h node motif, $F_{n_h,i}(h')$ is the n_h node motif fingerprint for node i, and $J_{h',i}$ is the number of occurrences of motif h' around node i. Given the fact that the functional network we set up earlier was undirected, we consider the motifs for $M = 3$, including 2 classes labeled as ID 1 and 2, and $M = 4$, including 6 classes labeled as ID 1 to 6. The schematic of the three-node and four-node motifs and its corresponding ID is shown in fig. 4. We compare the node motif fingerprint ($M = 3, 4$) between patients and control group by using one-way ANCOVA, and also join subject information including age, gender and education level (years) as covariates during the significance analysis.

In the significance analysis of the node motif fingerprint, we observe that in both classes of three-node motifs brain regions including the left middle frontal gyrus (MFG) (ID = 1: $p = 0.000002$/ID = 2: $p = 0.0001$), left anterior cingulate and paracingulate gyri (ACG) (ID = 1: $p = 0.0001$/ID = 2: $p = 0.0003$) and right PHG (ID = 1: $p = 0.0011$/ID = 2: $p = 0.0006$) show a marked difference between patients and control group. Other brain regions such as left ROL ($p = 0.0027$), right ACG ($p = 0.0013$), left PHG ($p = 0.0017$), right inferior parietal without supramarginal and angular gyri (IPL) ($p = 0.0009$) and bilateral thalamus (THA) (L: $p = 0.0001$/R: $p = 0.0001$)
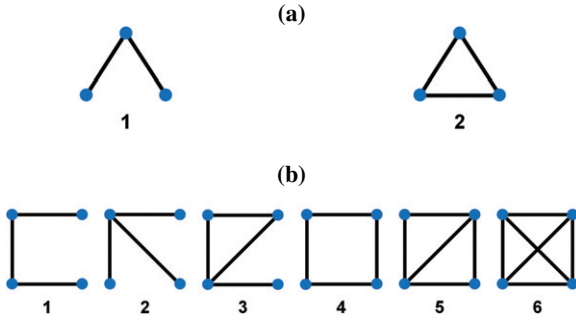
(a)

(b)

Fig. 4: The schematic of motifs and corresponding ID. (a) Three-node motif ID = 1 and 2. (b) Four-node motif ID = 1 to 6.

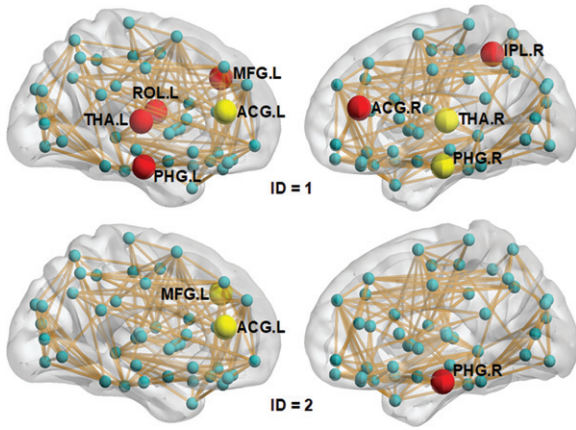

Fig. 5: Distributions of nodes showing significant network parameters differences ($p < 0.05$) under three-node motif. (MFG: middle frontal gyrus; ACG: anterior cingulate and paracingulate gyri; IPL: inferior parietal, but supramarginal and angular gyri; THA: thalamus).

Fig. 6: Distributions of nodes showing significant network parameters differences ($p < 0.05$) under four-node motif. (IFG-triang: inferior frontal gyrus; triangular part PAL: lenticular nucleus; pallidum ITG: inferior temporal gyrus).

also show similar properties in motif ID=1. The obtained significant brain regions with three-node motif ($M = 3$) are shown in fig. 5. In contrast to three-node motifs, most of the abnormal brain regions also show a significant difference in four-node motifs, such as left MFG and left ACG under motif ID = 1 to 5, right ACG and left THA under motif ID = 1, 2, 3 and 5, right THA under motif ID = 1 to 4, left PHG under motif ID = 2, 3 and 5, right PHG under motif ID = 3 and 5, right IPL under motif ID = 1 and 2, and finally left ROL under motif ID = 3. At the same time, some other brain regions also showed differences between groups in the four-node motif. Including the right inferior frontal gyrus of triangular part (IFGtriang) ($p = 0.0014$) and left pallidum in lenticular nucleus (PAL) ($p = 0.0031$) while motif ID = 1, right AMYG while motif ID = 3 ($p = 0.0045$) and 5 ($p = 0.0026$), left STG ($p = 0.0037$) and right inferior temporal gyrus (ITG) ($p = 0.0044$) while motif ID = 5. The obtained significant brain regions with four-node motif ($M = 4$) are shown in fig. 6.

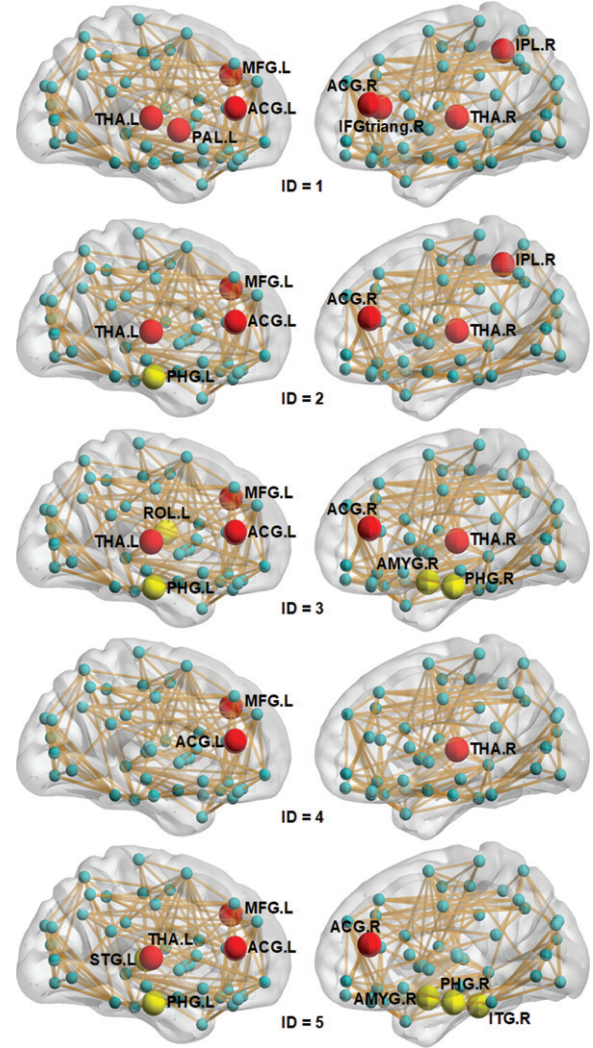Compared with the results of the clustering coefficient and shortest path length analysis we got before, the study

on the brain network motifs obtained some similar conclusions, that is, abnormalities occur in the left ROL, right PHG, right AMYG and left STG of the patient. While in the subnetwork edge analysis above, we can also find in the patient group that right PHG and right AMYG, which belong to the limbic structure, show significant differences compared to the control group. This further confirms that the dysfunction of the limbic system is closely related to the development of schizophrenia. Analysis of brain network motifs also lead to some important conclusions related to schizophrenia, such as changes around thalamus and cingulate gyrus. The thalamus is an important sensory relay station in cortically developed animals where nerve cells are replaced by sensory pathways throughout the body and then projected into the cerebral cortex. The functional connectivity to the thalamus was found reduced with insula, striatum and medial superior frontal

cortex and increased with sensory motor in schizophrenia [46,47], and, as a part of the limbic system, the cingulate gyrus has been reported to have reduced volume, altered neuronal arrangement, and anisotropy in diffusion tensor images [48]. We also find that in ID = 1 three-node motif, ACG, PHG and THA showed significant hemispheric asymmetry in the brain network. This asymmetry of functional connectivity was both found in schizophrenia patients and healthy controls through previous studies. However, the patients' asymmetry was attenuated, which develops with the disease duration and correlates with the psychotic symptoms. Present results also are in agreement with this phenomenon [49,50].

Conclusion. – In the present study, we apply MI to describe the correlation between brain regions and construct a whole brain level functional network to analyze the abnormal alterations of nodes and functional connections in patients with schizophrenia. We find that the abnormal brain areas are mainly located in the frontal temporal lobe regions. We also construct a subnetwork formed by the brain regions showing differences between the two groups to investigate the connectivity changes. By analyzing the difference of connectivity impairments in the subnetwork, we find a decreased edge strength among the impaired network nodes especially at limbic and frontal regions. Further motif analysis show regional network topological reorganizations in schizophrenia patients at limbic regions. There are some limitations in our study. First, the sample size is still relatively small, which needs to be further expanded to reach a more general conclusion. Second, there are still some limitations in the resolution of the 94 brain regions divided by the AAL2 template. Currently, there are some templates with a more detailed division of brain regions, and analysis based on these templates can achieve a more accurate localization of pathological regions. Finally, all patients included in our study are first-episode patients, which may be different from chronic patients. In future studies, this part of patients should also be included for comparison.

<p align="center">* * *</p>

REFERENCES

[1] White T. *et al.*, *Biol. Psychiatry*, **54** (2003) 418.
[2] Potkin S. G. *et al.*, *Schizophr. Bull.*, **35** (2008) 19.
[3] Marenco S. *et al.*, *Neuropsychopharmacology*, **37** (2012) 499.
[4] Baker J. T. *et al.*, *JAMA Psychiatry*, **71** (2014) 109.
[5] Cheng W. *et al.*, *NPJ Schizophr.*, **1** (2015) 15016.
[6] Whitfield-Gabrieli S. *et al.*, *Proc. Natl. Acad. Sci. U.S.A.*, **106** (2009) 1279.
[7] Palaniyappan L. *et al.*, *Neuron*, **79** (2013) 814.
[8] Jafri M. J. *et al.*, *Neuroimage*, **39** (2008) 1666.
[9] Majhi S. *et al.*, *Phys. Life Rev.*, **28** (2019) 100.
[10] Gao Z. *et al.*, *EPL*, **116** (2017) 50001.
[11] Xia C. *et al.*, *EPL*, **109** (2015) 58002.
[12] Gao Z. *et al.*, *IEEE Trans. Ind. Inform.*, **14** (2018) 3982.
[13] Gao Z. *et al.*, *Int. J. Bifurc. Chaos*, **27** (2017) 1750123.
[14] Gao Z. *et al.*, *Knowledge-Based Syst.*, **152** (2018) 163.
[15] Gao Z. *et al.*, *IEEE Trans. Instrum. Meas.*, **68** (2019) 2491.
[16] Zhang Y. *et al.*, *Schizophr. Res.*, **141** (2012) 109.
[17] van den Heuvel M. P. *et al.*, *J. Neurosci.*, **30** (2010) 15915.
[18] van den Heuvel M. P. *et al.*, *JAMA Psychiatry*, **70** (2013) 783.
[19] de Zwart J. A. *et al.*, *Neuroimage*, **47** (2009) 1649.
[20] Lahaye P.-J. *et al.*, *Neuroimage*, **20** (2003) 962.
[21] Maxim V. *et al.*, *Neuroimage*, **25** (2005) 141.
[22] Xie X. *et al.*, *Neuroimage*, **40** (2008) 1672.
[23] Lynall M.-E. *et al.*, *J. Neurosci.*, **30** (2010) 9477.
[24] Algunaid R. F. *et al.*, *Biomed. Signal Process.*, **43** (2018) 289.
[25] Jenkinson M. *et al.*, *Neuroimage*, **62** (2012) 782.
[26] Cox R. W., *Comput. Biomed. Res.*, **29** (1996) 162.
[27] Rolls E. T. *et al.*, *Neuroimage*, **122** (2015) 1.
[28] Wei Y. *et al.*, *Hum. Brain Mapp.*, **38** (2017) 2734.
[29] Rubinov M. and Sporns O., *Neuroimage*, **52** (2010) 1059.
[30] van den Heuvel M. P. and Sporns O., *Trends Cogn. Sci.*, **17** (2013) 683.
[31] Cavanna A. E. and Trimble M. R., *Brain*, **129** (2006) 564.
[32] Faget-Agius C. *et al.*, *J. Psychiatry Neurosci.*, **37** (2012) 297.
[33] Kühn S. and Gallinat J., *Schizophr. Bull.*, **39** (2011) 358.
[34] Battaglia F. P. *et al.*, *Trends Cogn. Sci.*, **15** (2011) 310.
[35] Heckers S. and Konradi C., *Hippocampal pathology in schizophrenia*, in *Behavioral Neurobiology of Schizophrenia and its Treatment* (Springer) 2010, pp. 529–553.
[36] Heckers S. and Konradi C., *Schizophr. Res.*, **167** (2015) 4.
[37] Grace A. A., *Nat. Rev. Neurosci.*, **17** (2016) 524.
[38] Stegmayer K. *et al.*, *Schizophr. Bull.*, **44** (2017) 359.
[39] Eack S. M. *et al.*, *PLoS One*, **11** (2016) e0149297.
[40] Minzenberg M. J. *et al.*, *Arch. Gen. Psychiatry*, **66** (2009) 811.
[41] Fornito A. *et al.*, *Biol. Psychiatry*, **70** (2011) 64.
[42] Achard S. and Bullmore E., *PLoS Comput. Biol.*, **3** (2007) e17.
[43] Guo S. *et al.*, *Hum. Brain Mapp.*, **35** (2014) 123.
[44] Joshi D. *et al.*, *Biol. Psychiatry*, **72** (2012) 725.
[45] Lee S.-H. *et al.*, *Schizophr. Bull.*, **42** (2015) 790.
[46] Anticevic A. *et al.*, *Cereb. Cortex*, **24** (2013) 3116.
[47] Woodward N. D. and Heckers S., *Biol. Psychiatry*, **79** (2016) 1016.
[48] Segal D. *et al.*, *Neuroimage*, **50** (2010) 357.
[49] Jalili M. *et al.*, *Psychophysiology*, **47** (2010) 706.
[50] Ribolsi M. *et al.*, *Front. Hum. Neurosci.*, **8** (2014) 1010.